Role of phase-dependent influence function in the Winfree model of coupled oscillators

M. Manoranjani,[1] R. Gopal,[1] D. V. Senthilkumar,[2,*] and V. K. Chandrasekar[1,†]

[1]*Department of Physics, Centre for Nonlinear Science and Engineering, School of Electrical and Electronics Engineering, SASTRA Deemed University, Thanjavur 613401, India*

[2]*School of Physics, Indian Institute of Science Education and Research, Thiruvananthapuram 695016, India*

(Received 21 July 2021; revised 11 October 2021; accepted 24 November 2021; published 10 December 2021)

We consider a globally coupled Winfree model comprised of a phase-dependent influence function and sensitive function, and unravel the impact of offset and integer parameters, characterizing the shape of the influence function, on the phase diagram of the Winfree model. The decreasing value of the offset parameter decreases the degree of positive phase shift among the oscillators by promoting the negative phase shift, which indeed favors the onset of multistability among the synchronous oscillatory state and asynchronous stable steady states in a large region of the phase diagram. Further, large integer parameters lead to brief pulses of the influence function, which again enhances the effect of the offset parameter. There is an explosive transition to a synchronous oscillatory state from an asynchronous steady state via a Hopf bifurcation. Dynamical transitions and multistability emerge through saddle-node, pitchfork, and homoclinic bifurcations in the phase diagram. We deduce two ordinary differential equations corresponding to the two macroscopic variables from the population of globally coupled Winfree oscillators using the Ott-Antonsen ansatz. We also deduce various bifurcation curves analytically from the reduced low-dimensional macroscopic variables for the exactly solvable case. The analytical curves exactly match the simulation boundaries in the phase diagram.

DOI: 10.1103/PhysRevE.104.064206

I. INTRODUCTION

In 1967, Winfree proposed a theoretical model to investigate the spontaneous synchronization of a large population of biological oscillators despite their heterogeneity [1–3]. In its simplest form, the model is comprised of phase oscillators with intrinsic natural frequency and the interaction among the oscillators modeled by a phase-dependent influence function and a sensitive function, determining the response of individual oscillators to the mean field. The influence function is usually in the form of a pulse, while the mathematical form of the sensitive function can be chosen such that it is consistent with the qualitative shape of the phase-response curve of certain biological oscillators. Hence, the phase-dependent sensitive function is also referred to as a phase-response curve (PRC) [4–8]. With these settings, the Winfree model is a unique model representing a class of pulse-coupled biological oscillators [9–11]. Familiar examples for pulselike interactions include flashing of fireflies [12], applauding audiences [13], and action potentials of neurons [14].

A detailed phase diagram of the original Winfree model is yet to be explored as it is very difficult to analyze mathematically in its most general form. Nevertheless, a detailed bifurcation analysis of the model for a special tractable case of pulse-coupled oscillators has been provided by Ariaratnam and Strogatz [5] in terms of phase diagrams. Incoherence, frequency locking, and death states along with the multistability among these states were classified in the phase space of coupling strength and frequency distribution. Since then, a phase diagram of the Winfree model has been the object of investigation, but with limited success [4,6,7,15,16]. Renewed interest in the theoretical analysis of populations of phase oscillators arose due to Ott and Antonsen's report on an exact dimensionality reduction of the infinite-dimensional Kuramoto oscillator, leading to the Ott-Antonsen ansatz [17,18].

Surprisingly, the Ott-Antonsen ansatz is shown to be applicable to the pulse-coupled oscillators [4,7]. This development has opened up the possibility of investigating macroscopic dynamical states peculiar to the Winfree model and its variants, which are far from reachable using the Kuramoto or Kuramoto-like oscillators. In particular, the Winfree model has the advantage of describing different sets of pulse-coupled biological oscillators [2,19] and disseminating the influence of various pulse shapes and phase-response curves on the macroscopic synchronization. Specifically, understanding the underlying dynamical aspects of the Winfree model will shed more light on the observed biological phenomena using mathematical models.

The dynamics of the Winfree model with a sinusoidal PRC is shown to evolve into the so-called Ott-Antonsen manifold by reducing the high-dimensional system into two ordinary differential equations corresponding to two macroscopic variables [7]. In particular, Pazó *et al.* exhaustively explored the effect of the shape of the phase-response curves and their pulse width on the collective dynamics. Brief pulses are found to facilitate the synchronization of heterogeneous oscillators,

*skumar@iisertvm.ac.in
†chandru25nld@gmail.com

a phenomenon that cannot be observed with broad pulses. Further, the effect of brief pulses is found to be largely enhanced as the PRC is made more off-centered. A variety of chimera states has also been established in a network of pulse-coupled oscillators. Recently, a variety of pulse shapes and sinusoidal PRCs have been employed to investigate their effects in the phase diagram and synchronization [4]. It was revealed that brief pulses favoring the synchronization of heterogeneous oscillators do not hold for negative PRC offsets, which are asymmetric. Instead, in this case, an intermediate pulse width was shown to facilitate the macroscopic synchronization of heterogeneous oscillators. Further, the synchronization scenario is found to heavily depend on the particular pulse type.

In this work, we systematically analyze the impact of the phase-dependent influence function on the synchronization transition of the Winfree model. We deduce two ordinary differential equations corresponding to the two macroscopic variables from the population of globally coupled Winfree oscillators using the Ott-Antonsen ansatz. In particular, we investigate the influence of the offset parameter and the width of the phase-dependent influence function on the phase diagram of the globally coupled Winfree model. The phase-dependent influence function either advances or delays the phase shift of the oscillators based on the offset parameter. Dynamical transitions among the asynchronous steady states and synchronous oscillatory state onset via Hopf, pitchfork, saddle-node, and homoclinic bifurcations in the phase diagram of the Winfree oscillators. Further, there emerges a first-order (explosive) transition to the synchronized oscillatory state in the multistable region. We find that brief pulses and decreasing degree of phase advance, characterizing the influence function, favor the onset of a multistable region and explosive transition to a synchronous oscillatory state in a large range of the phase diagrams. We obtain the distinct bifurcation curves using the software XPPAUT for nonzero values of the offset parameter. Nevertheless, we deduce the bifurcation curves analytically for the null value of the offset parameter as the reduced low-dimensional macroscopic system of equations can be solved exactly. We also find that the analytical curves match exactly with the simulation boundaries.

The plan of the paper is as follows. In Sec. II, we introduce the Winfree model along with the intricacies of the phase-dependent influence function and the sensitive function. We deduce the low-dimensional dynamics of the globally coupled Winfree model using the Ott-Antonsen ansatz in Sec. III. Further, we also present the phase diagrams of the Winfree model for distinct values of the offset parameter and the integer parameter, characterizing the width of the influence function, in Sec. IV. Finally, we provide a brief summary of our results in Sec. V.

II. GENERALIZED WINFREE MODEL

The Winfree model is governed by the evolution equation represented as [1,3]

$$\dot{\theta}_i = \omega_i + Q(\theta_i)\frac{\varepsilon}{N}\sum_{j=1}^{N} P(\theta_j), \quad i = 1, 2, 3, \ldots, N, \tag{1}$$

where $\theta_i(t)$ is the phase of the ith oscillator and $\varepsilon > 0$ is the coupling strength. $Q(\theta)$ and $P(\theta)$ in the coupling measure the sensitivity and influences of all oscillators, respectively. The frequencies ω_i, which are drawn from a symmetric and unimodal density function $g(\omega)$, ensure the heterogeneous nature of the oscillators. All the oscillators receive the common input via the mean-field coupling $\frac{1}{N}\sum_{j=1}^{N} P(\theta_j)$. The response of the individual oscillators to the mean-field depends on the state of each oscillator θ_i, which is determined by the sensitivity function $Q(\theta_i)$. Usually, the specific choice of the latter is $Q(\theta) = -\sin\theta$ [5], which is chosen for its mathematical tractability and is also consistent with the qualitative shape of the response curves of a large class of biological oscillators [1,2]. It is to be noted that the effect of heterogeneous PRCs [8], noninfinitesimal PRCs [20], and various forms of pulses including different degree of pulse width [4] on synchronization have been reported recently. The phase-dependent influence function $P(\theta)$ characterizes the nature of the pulse, which is usually considered as $(1 + \cos\theta)^n$ [5,7]. The Winfree model with this kind of influence function represents a simple model of a population of pulse-coupled biological oscillators [7,21]. In our present study, we consider the phase-dependent influence function $P(\theta)$ of the form

$$P(\theta) = a_n(q + \cos\theta)^n, \tag{2}$$

where $P(\theta)$ is a 2π-periodic pulselike function characterized by the offset parameter q. The phase-dependent influence function $P(\theta)$ either advances or delays the phase shift of the oscillators based on the offset parameter q. $P(\theta)$ is completely positive [see dashed curve in Fig. 1(a) for $n = 1$] for the unit value of q characterizing phase advance. A decreasing value of q decreases the degree of phase advance because of the contribution from phase delay [see Figs. 1(b) and 1(c) for $q = 0.9$ and 0.3, respectively] and becomes perfectly balanced when the offset parameter takes the null value. Nevertheless, the instantaneous value of $P(\theta_j)$ depends on the distribution of θ_j, which evolves in concurrence with the distribution of the natural frequencies and the sensitive function (PRC). The integer parameter n permits us to control the width of the pulses. The normalization constant a_n is fixed, in accordance with $\int_{-\pi}^{\pi} P(\theta)d\theta = 2\pi$, as $a_n^{-1} = \sum_{m=0}^{n} \binom{n}{m} \frac{(q-1)^m (2(n-m))!}{2^{n-m}((n-m)!)^2}$ [7]. The phase-dependent influence function is depicted in Fig. 1 for $n = 1$ (dashed line) and $n = 10$ (solid line) to elucidate the influence of n on the width of the pulses, which becomes increasingly narrow for large values of n.

The heterogeneity among the population is obtained through a Lorentzian distribution of ω_i with mean ω_0 and spread γ, represented as

$$g(\omega) = \frac{\gamma}{\pi[(\omega - \omega_0)^2 + \gamma^2]}; \ \gamma > 0. \tag{3}$$

III. LOW-DIMENSIONAL DYNAMICS OF THE WINFREE MODEL

In this section, we reduce a low-dimensional system representing the mean-field dynamics of the Winfree model (1) in the thermodynamic limit. The Winfree model, for the chosen form of the influence and response functions, can be written

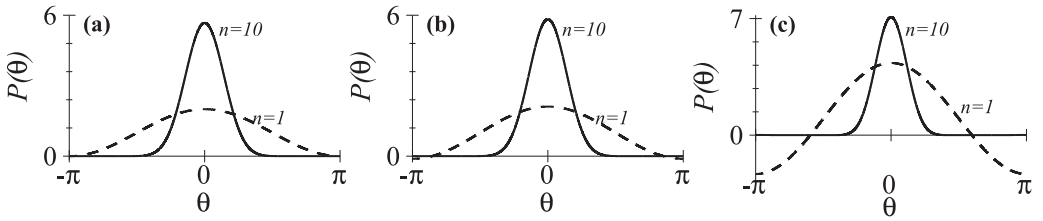

FIG. 1. Phase-dependent influence function for various values of the offset parameter. (a) $q = 1$, (b) $q = 0.9$, and (c) $q = 0.3$.

as

$$\dot{\theta}_i = \omega_i + \varepsilon \mathrm{Im}[e^{-i\theta_i}]H(t), \tag{4}$$

where $H(t) = \sum P(\theta_i)$, and the order parameter $z(t) = r(t)e^{i\psi} = \frac{1}{N}\sum_{j=1}^{N} e^{i\theta_j}$. For a large but finite N, the above system of equations admits solutions in the reduced invariant Ott and Antonsen manifold [17], provided the frequencies ω_i are drawn from a probability distribution function such as Lorentzian or Gaussian functions [7,18,22]. Now, we proceed to deduce the low-dimensional system that captures the asymptotic dynamics of the Winfree model (1) using the Ott-Antonsen (OA) ansatz.

We consider a density function f represented as $f(\theta, \omega, \gamma)d\theta$, which denotes a fraction of the oscillators with phases between θ and $\theta + d\theta$ and natural frequency ω at a time t. The evolution of f is governed by the continuity equation

$$\frac{\partial f}{\partial t} + \frac{\partial}{\partial \theta}(fv) = 0, \tag{5}$$

where $v(\theta, \omega, t)$ is the angular velocity of the oscillators given by Eq. (4). For further analysis, in the thermodynamic limit, $z(t)$ can be written as

$$z(t) = \int_{-\infty}^{\infty} g(\omega) \int_0^{2\pi} f(\theta, \omega, t)e^{i\theta} d\theta d\omega. \tag{6}$$

Expanding $f(\theta, \omega, t)$ in Fourier series (since it is 2π periodic) in θ, we have

$$f(\theta, \omega, t) = \frac{g(\omega)}{2\pi}\left[1 + \sum_{l=1}^{\infty} f_l(\omega, t)e^{il\theta} + \text{c.c.}\right], \tag{7}$$

where c.c. stands for the complex conjugate of the preceding sum.

The OA ansatz assumes [17,18]

$$f_l(\omega, t) = [\alpha(\omega, t)]^l. \tag{8}$$

Substituting (7) and (8) in the continuity equation, one obtains

$$\dot{\alpha} + i\omega\alpha - \frac{\varepsilon}{2}H(1 - \alpha^2)a_n = 0. \tag{9}$$

Hence, Eq. (6) can be written as

$$z(t) = \int_{-\infty}^{\infty} g(\omega)\alpha^*(\omega, t)d\omega. \tag{10}$$

The above equation can be integrated to obtain

$$z(t) = \alpha^*(\omega_0 - i\gamma, t). \tag{11}$$

From (9) and (11), the dynamics of the Kuramoto order parameter $z(t) = re^{i\psi}$ can be deduced as

$$\dot{r} = -\gamma r + \frac{k}{2}(1 - r^2)\cos(\psi)[(r\cos\psi + q)^n], \tag{12a}$$

$$\dot{\psi} = \omega_0 - \frac{k}{2}\frac{(1 + r^2)}{r}\sin(\psi)[(r\cos\psi + q)^n], \tag{12b}$$

where $k = \varepsilon a_n$. Remarkably, the above two equations describe exactly the macroscopic dynamics of the Winfree model (1), irrespective of the presence of the offset parameter in the influence function.

IV. PHASE DIAGRAM OF THE WINFREE MODEL

In this section, we unravel the phase diagram of the Winfree model (1) for different values of the offset parameter q and the integer parameter n, which controls the symmetry and the width of the phase-dependent influence function $P(\theta)$, respectively. First, we solve the original Winfree model (1) to identify the synchronous and asynchronous states in the $(\omega_0/\gamma, k/\gamma)$ parameter space using the order parameter ξ. The reduced low-dimensional system (12), corresponding to the macroscopic dynamics of the Winfree model (1), cannot be solved exactly for nonzero values of the offset parameter. However, using the XPPAUT software [23], we have obtained the bifurcation curves in the two parameter space for nonzero values of the offset parameter. Nevertheless, we have solved the low-dimensional system for $q = 0$ to deduce various bifurcation curves.

A. Phase diagram of the Winfree model for $q \neq 0$

The macroscopic synchronized state is characterized by the periodic nature of $|z|$ in the thermodynamic limit, while that of the asynchronized state is characterized by $|z| = \text{const}$. Hence, we use the Shinomoto-Kuramoto order parameter [4,24]

$$\xi = \overline{|z - \bar{z}|}, \tag{13}$$

where $\bar{z}$ denotes the long time average. The Shinomoto-Kuramoto order parameter takes $\xi = 0$ for the asynchronized state, whereas nonzero values of ξ characterize the degree of synchronization. We have employed the standard fourth-order Runge-Kutta algorithm with a time step $h = 0.01$, $N = 10^5$, $\gamma = 0.1$ and the initial conditions of the phase variables are chosen randomly between $[0, 2\pi)$. Based on the values of the Shinomoto-Kuramoto order parameter, $(\omega_0/\gamma, k/\gamma)$ parameter space is demarcated as synchronous (light-gray and black regions) and asynchronous (unshaded and dark-gray regions) regions in Fig. 2 for $n = 1$. The phase diagram for $q = 1$ is depicted in Fig. 2(a). There is a transition from

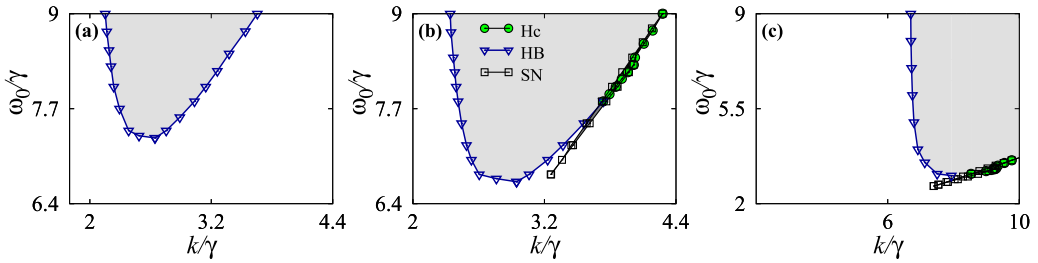

FIG. 2. Phase diagram of the Winfree model (1) in the $(\omega_0/\gamma, k/\gamma)$ parameter space for different values of the offset parameter q. (a) $q = 1$, (b) $q = 0.9$, and (c) $q = 0.3$.

an asynchronous stable steady state to a synchronous oscillatory state, and then again to an asynchronous state as a function of k/γ for $\omega_0/\gamma > 7.2$. The line connected by unfilled triangles corresponds to the Hopf bifurcation curve (obtained using XPPAUT) across which a change in the stability of the stable steady state of the reduced low-dimensional system (12) occurs. Now, we decrease the value of the offset parameter q to unravel its effect on the dynamical states of the Winfree model. Note that decreasing q decreases the degree of positive phase shift (phase advance) among the oscillators as characterized by the phase-dependent influence function $P(\theta)$ (see Fig. 1). The phase diagram for $q = 0.9$ is shown in Fig. 2(b). In addition to the Hopf bifurcation observed for $q = 1$, decreasing q facilitates the onset of homoclinic and saddle-node bifurcations enclosing the multistable regions in a narrow range of parameters. It is also to be noted that decreasing the offset parameter favors the onset of synchronization in a large parameter space [Fig. 2(b)]. Further decrease in q increases the synchronized and multistable regions as evident from Figs. 2(c) and 3 depicted for $q = 0.3$. The multistable region in Fig. 2(c) is enlarged in Fig. 3 for a clear visualization and better understanding of the dynamical transitions in the multistable region. For low values of ω_0/γ (see Fig. 3), two fixed points coexist in the dark-gray shaded region, while a synchronized oscillatory state coexists with the steady state in the dark (black) shaded region in the range $\omega_0/\gamma \in (3.1, 3.6)$. A second nontrivial steady state onsets via the saddle-node bifurcation (line connected by unfilled squares) and remains stable, as a function of k/γ in the entire parameter space, resulting in the multistability among the two different nontrivial steady states. However, the steady state that lies to the left of the saddle-node bifurcation curve loses its stability at a subsequent saddle-node bifurcation (line connected by unfilled squares) for further larger k/γ. The synchronized oscillatory state destabilizes via homoclinic bifurcation for $\omega_0/\gamma > 3.1$, leading to the onset of a nontrivial steady state as a function of k/γ.

Phase-space trajectories near the stable nontrivial steady states and that of the limit-cycle attractor are illustrated in the inset of Fig. 3. Stable (unstable) steady states are indicated by unfilled (filled) symbols in Figs. 3 and 4. Phase-space trajectories near the two stable nontrivial steady states that coexist in the dark-gray region in Fig. 3 and phase-space trajectories near the stable limit-cycle attractor and stable nontrivial steady state that coexist in the dark (black) shaded region in Fig. 3 are shown in Figs. 4(a) and 4(b), respectively. The Shinomoto-Kuramoto order parameter ξ is depicted in Fig. 5 for two different q and ω_0 to illustrate the nature of dynamical transitions observed in the phase diagrams of Fig. 2. The Shinomoto-Kuramoto order parameter ξ is widely used in identifying the synchronization transition in the Winfree models [4,7]. The order parameter in Fig. 5(a), plotted for $q = 1$ and $\omega_0 = 0.85$, elucidates the transition from an asynchronous steady state to synchronous oscillatory state at $k/\gamma = 2.2$ via the Hopf bifurcation and, subsequently, the latter is quenched to an asynchronous stable steady state again

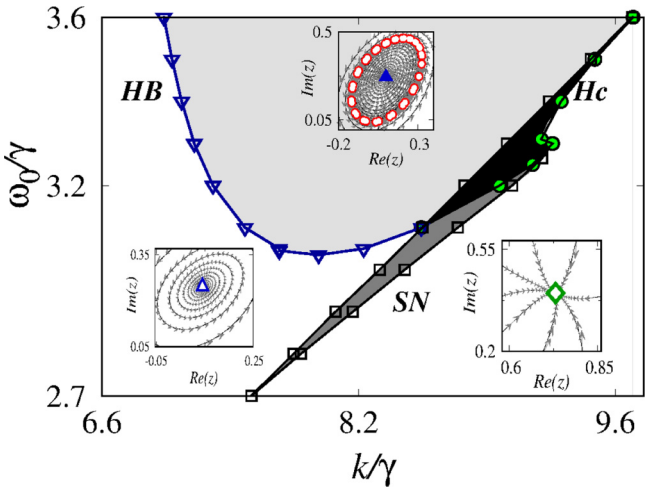

FIG. 3. Enlarged region of Fig. 2(c). Stable nontrivial steady states are indicated by unfilled symbols, whereas the unstable trivial steady state is indicated by a filled symbol in the inset. Phase-space trajectories near the stable nontrivial steady states and the limit-cycle attractor (unfilled circles) are depicted in the inset.

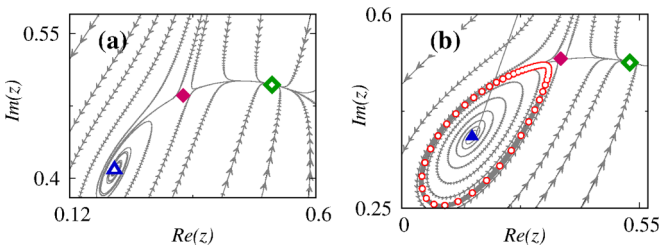

FIG. 4. Phase-space trajectories near (a) the nontrivial steady states in the dark-gray shaded region in Fig. 3 and (b) the limit-cycle attractor and the nontrivial steady states in the dark-shaded region in Fig. 3, for $q = 0.3$. Stable states are shown using unfilled symbols and unstable states using filled symbols.

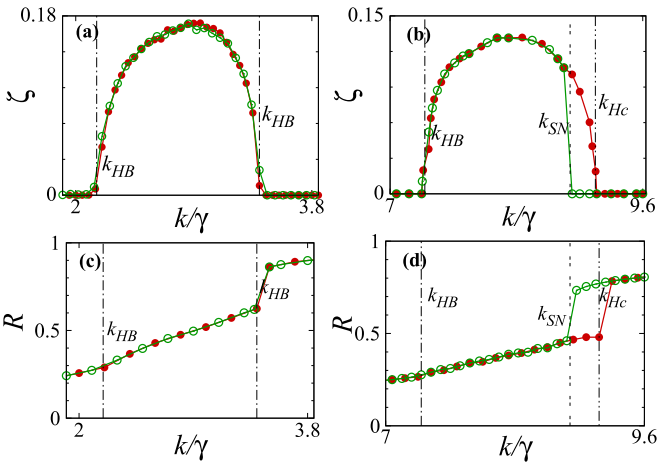

FIG. 5. Shinomoto-Kuramoto order parameter (ξ) and Kuramoto order parameter (R) illustrating the nature of dynamical transitions. (a), (c) $q = 1$, $\omega_0 = 0.85$; (b), (d) $q = 0.3$, $\omega_0 = 0.32$.

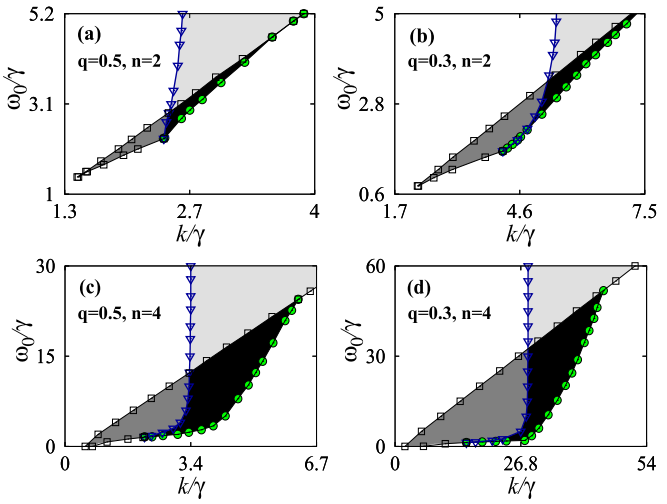

FIG. 6. Phase diagram of the Winfree model (1) and (2) for different pulse width and offset parameters. (a) $n = 2$, $q = 0.5$; (b) $n = 2$, $q = 0.3$; (c) $n = 4$, $q = 0.5$; and (d) $n = 4$, $q = 0.3$.

via the Hopf bifurcation at $k/\gamma = 3.4$. The entire dynamical transition, illustrated in Fig. 5(a), is a cross section of Fig. 2(a) at $\omega_0/\gamma = 8.5$. Lines connected by filled and open circles correspond to the forward and backward trace of k/γ. Interestingly, we have observed a first-order (explosive) transition to the synchronous oscillatory state in the multistable regions of Figs. 2(b) and 2(c). For instance, the order parameter ξ for $q = 0.3$ and $\omega_0 = 0.32$ [see Fig. 5(b)] in the forward transition elucidates that there is a transition from an asynchronous steady state to a synchronous oscillatory state at $k/\gamma = 7.2$ via the Hopf bifurcation, which loses its stability via a homoclinic bifurcation at $k/\gamma = 9.2$ leading to the onset of an asynchronous stable steady state. Nevertheless, one can observe a first-order transition, similar to an explosive transition, from an asynchronous stable steady state to a synchronous oscillatory state via a saddle-node bifurcation at $k/\gamma = 8.9$ in the backward transition, which then is quenched to a stable steady state at $k/\gamma = 7.2$ via the Hopf bifurcation. Thus, it is also evident that in the multistable regions, there is a first-order (explosive) transition to the synchronized oscillatory state in the backward transition.

We have also depicted the Kuramoto order parameter $R = \overline{|z|}$ in Figs. 5(c) and 5(d) for the same values of the parameters as in Figs. 5(a) and 5(b), respectively, to doubly confirm the dynamical transitions observed in the Shinomoto-Kuramoto order parameter ξ. The Kuramoto order parameter R clearly reveals the transition among the asynchronous states (stable nontrivial steady states) via a synchronized (oscillatory) state [see Figs. 5(c) and 5(d)] through similar bifurcations as in Figs. 5(a) and 5(b). Note that there exists a region of bistability [see Fig. 5(d)] with the first-order transition in both the forward and backward trace of k/γ. We have also increased the integer parameter n, which basically narrows down the phase-dependent influence function as illustrated in Fig. 1, and depicted the corresponding phase diagrams in Figs. 6 and 7 to elucidate the effect of the brief influence function $P(\theta)$ on the dynamical states. We have fixed $n = 2$ and depicted the phase diagrams for $q = 0.5$ and $q = 0.3$ in Figs. 6(a) and 6(b), respectively. The dynamical transitions via distinct bifurcations are similar to those in Fig. 2(d). Similarly, we have also depicted the phase diagrams for $n = 4$ in Figs. 6(c) and 6(d) for $q = 0.5$ and $q = 0.3$, respectively. The phase diagrams for odd values of n for $q = 0.5$ and $q = 0.3$ are shown in Figs. 7. It is evident from these figures that the spread of the multistable states is increased for the decreasing values of the offset parameter and increasing values of n. These figures corroborate that brief pulses and decreasing degree of phase advance characterized by the influence function $P(\theta)$ favor the onset of multistable regions and explosive transition to a synchronous oscillatory state in a large range in the phase diagrams.

B. Phase diagram of the Winfree model for $q = 0$

In this section, we investigate the dynamical states and the nature of the phase-space dynamics of the Winfree model for $q = 0$ and $n = 1$, the phase diagram of which is depicted

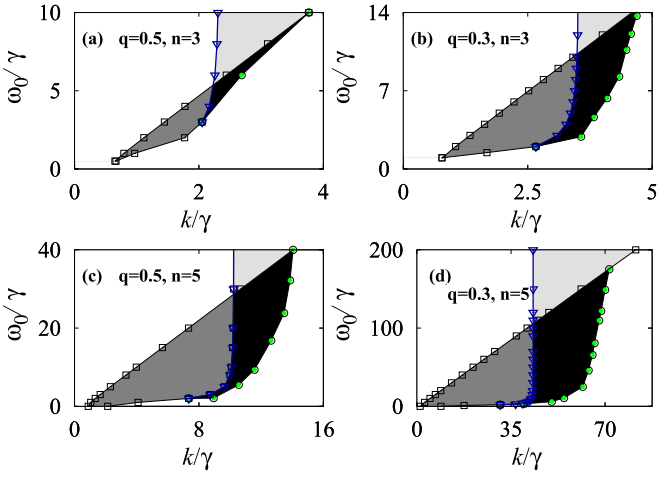

FIG. 7. Phase diagram of the Winfree model (1) and (2) for different pulse width and offset parameter. (a) $n = 3$, $q = 0.5$; (b) $n = 3$, $q = 0.3$; (c) $n = 5$, $q = 0.5$; and (d) $n = 5$, $q = 0.3$.

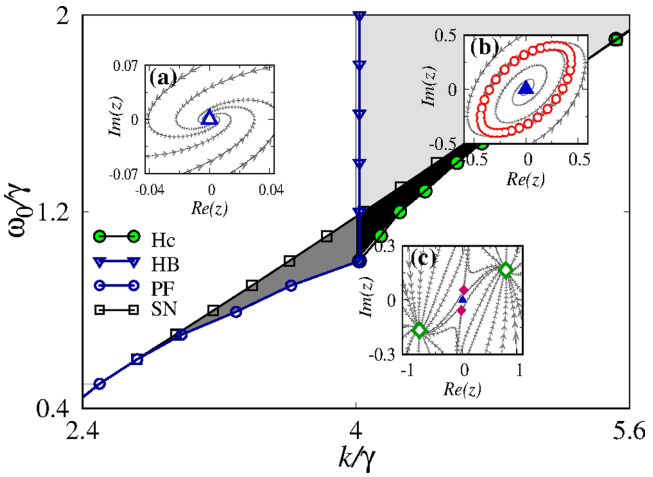

FIG. 8. Phase diagram of the Winfree model for $q = 0$ and $n = 1$.

in Fig. 8. Note that for $n = 1$, the normalization constant $a_1 = 1/q \to \infty$ for $q \to 0$. For this reason, we have fixed $k = \varepsilon$ in this section instead of $k = \varepsilon a_1$. The asynchronous steady state to the left of the Hopf bifurcation curve (line connected by unfilled triangles) and that lie above the pitchfork bifurcation curve (line connected by unfilled circles) correspond to the trivial stable steady state. The trajectories near the trivial steady state elucidating its stable nature are shown in the Fig. 8(a) inset. Note that stable states are shown using unfilled symbols, while unstable states are shown using filled symbols. The asynchronous steady state that lies to the right of the saddle-node bifurcation curve (line connected by unfilled squares) is a nontrivial stable steady state. The trajectories near the stable nontrivial steady state (indicated as an open square) are shown in the Fig. 8(c) inset. The essential differences between the phase diagrams in the presence and absence of an offset parameter are the emergence of a stable trivial steady state and loss of its stability via the pitchfork bifurcation as a function of k/γ. The synchronous oscillatory state is enclosed between the Hopf bifurcation curve and the homoclinic bifurcation curve (line connected by filled circles). Stable limit-cycle oscillation (indicated by open circles) of the synchronous oscillatory state is shown in the Fig. 8(b) inset. The trivial steady state and nontrivial steady state coexist in the dark-gray shaded region enclosed by the saddle-node bifurcation curve and the pitchfork bifurcation curve. Phase trajectories near both trivial and nontrivial steady states are depicted in Fig. 9(a). Synchronous oscillatory and asynchronous nontrivial steady states coexist in the dark (black) shaded region enclosed by the saddle-node bifurcation curve and the homoclinic bifurcation curve. Phase trajectories near the stable limit-cycle oscillation and that of the nontrivial steady states are shown in Fig. 9(b). Note that there is also an explosive transition to a synchronous oscillatory state from an asynchronous nontrivial steady state as in Fig. 2(c). It is also to be noted that all the bifurcation curves in Fig. 8, except the homoclinic bifurcation curve, are analytical bifurcation curves deduced from the reduced low-dimensional system (12), corresponding to the macroscopic dynamics of the Winfree model (1). The reduced low-dimensional system can now be exactly solvable for $q = 0$ and $n = 1$. In the following, we

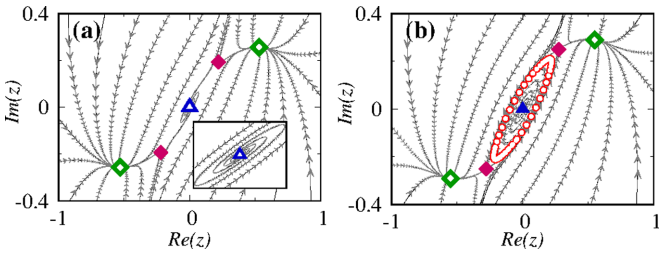

FIG. 9. Phase-space trajectories near (a) trivial and nontrivial steady states and (b) limit-cycle and nontrivial steady states. Stable states are shown using unfilled symbols and unstable states using filled symbols.

will deduce the critical curves corresponding to the distinct bifurcations.

1. Stability of trivial steady state

The reduced low-dimensional system (12) is characterized by a trivial steady state ($r = 0$) and a nontrivial steady state ($r \neq 0$). The stability determining the eigenvalues of the trivial steady state is

$$\lambda_{1,2} = -4\gamma + k \pm \sqrt{\Delta}, \tag{14}$$

where $\Delta = k^2 - 16\omega_0^2$. For $\frac{\omega_0}{\gamma} \leqslant 1$, the critical curve (pitchfork bifurcation curve) across which the stability of the stable trivial steady state switches can be deduced as

$$k_{PF} = \frac{2\left(\gamma^2 + \omega_0^2\right)}{\gamma}. \tag{15}$$

For $\frac{\omega_0}{\gamma} > 1$, the stable trivial steady state loses its stability via the Hopf bifurcation curve,

$$k_{HB} = 4. \tag{16}$$

2. Stability of nontrivial steady state

The nontrivial steady state is obtained by substituting $\dot{r} = \dot{\psi} = 0$ in Eqs. (12), which yields

$$\cos\psi = \sqrt{\frac{2\gamma}{k(1-r^2)}} \tag{17}$$

and

$$\sin\psi = \frac{\sqrt{\frac{2}{k\gamma}}\omega_0\sqrt{(1-r^2)}}{1+r^2}. \tag{18}$$

The above two equations can be rewritten as

$$\frac{2\gamma}{k(1-r^2)} + \frac{2(1-r^2){\omega_0}^2}{\gamma k(r^2+1)^2} = 1. \tag{19}$$

The above equation can be reduced to

$$\gamma k R^3 + R^2\left(2\gamma^2 + \gamma k + 2\omega_0^2\right) + R\left(4\gamma^2 - \gamma k - 4\omega_0^2\right) + 2\omega_0^2 + 2\gamma^2 - \gamma k = 0, \tag{20}$$

where $R = r^2$. Now, from the discriminant of the above cubic equation, the existence condition for the nontrivial steady

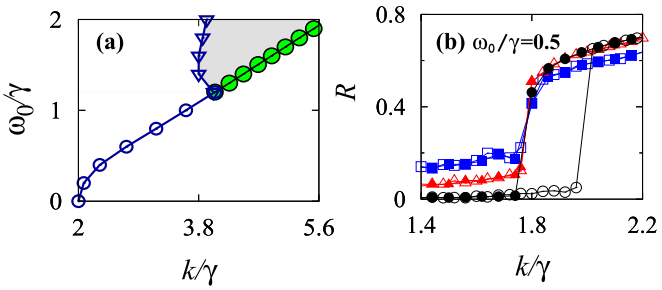

FIG. 10. (a) Phase diagram of the Winfree model for $N = 100$, and (b) Kuramoto order parameter R for $N = 100$ (lines connected by squares), 1000 (lines connected by triangles), and 10^5 (lines connected by circles) at $\omega_0/\gamma = 0.5$. Filled and unfilled symbols correspond to the forward and backward traces of k/γ. The other parameters are $q = 0$ and $n = 1$.

state, which genesis is via the saddle-node bifurcation, can be deduced as

$$4\gamma k_{SN}^3 + k_{SN}^2(\omega^2 - 12\gamma^2) + 4k_{SN}(3\gamma^3 - 5\gamma\omega^2) - 4(\gamma^2 + \omega^2)^2 = 0. \quad (21)$$

The existence condition of the nontrivial steady state turns out to be its stability condition, which can be verified independently. The saddle-node bifurcation curve bifurcates from the pitchfork bifurcation curve at $\frac{\omega_0}{\gamma} = \frac{1}{\sqrt{3}}$, leading to the onset of multistability among the trivial and nontrivial steady states.

V. FINITE-SIZE EFFECTS

We have also depicted the Kuramoto order parameter and the phase diagram for small values of N to elucidate the finite-size effects on the observed dynamical states and their transitions. In particular, the phase diagram for $N = 100$ is depicted in Fig. 10(a). The values of the other parameters in Figs. 10(a) and 10(b) are the same as in Fig. 8. The dynamical states and their bifurcation transitions are similar to those in Fig. 8 for $N = 10^5$, except for the absence of bistability among the observed dynamical states. The Kuramoto order parameter is depicted in Fig. 10(b) for $N = 100$ (lines connected by squares), 1000 (lines connected by triangles), and 10^5 (lines connected by circles) at $\omega_0/\gamma = 0.5$. Filled and unfilled symbols correspond to the forward and backward traces of k/γ, respectively. It is evident from the figure that the first-order transition across the bistable region is observed only for a very large N, which is otherwise absent for a small N. Thus, bistability and the first-order (explosive) transition among the dynamical states onsets only for a large but finite N.

VI. CONCLUSIONS

We considered a globally coupled Winfree model comprised of a phase-dependent influence function and sensitive function, in which all the oscillators interact through the mean field of the influence function while the degree of response of the individual oscillators to the mean field is determined by the sensitive function. We have investigated the influence of the offset and integer parameters characterizing the shape of the phase-dependent influence function. The increasing phase delay facilitated the onset of multistable regions in the phase diagram. Multistability between the synchronous oscillatory state and asynchronous stable steady states is enclosed by the saddle-node bifurcation and homoclinic bifurcation. Multistability is also found to emerge between two nontrivial steady states bounded by two saddle-node bifurcations for nonzero values of the offset parameter. Furthermore, a trivial steady state and nontrivial steady states are found to coexist in the region bounded by the saddle-node bifurcation and the pitchfork bifurcation in the phase diagram in the absence of the offset parameter.

Increasing the integer parameter results in a brief pulse of the phase-dependent influence function, which is also found to facilitate the emergence of a synchronous oscillatory state and multistable states to a large range of the phase diagram. An explosive transition to a synchronous oscillatory state from the asynchronous steady state is found to emerge in the backward transition. In particular, decreasing phase advance and brief pulses of the influence function are found to promote synchronization among the heterogeneous oscillators. We have also deduced two ordinary differential equations corresponding to the two macroscopic variables from the population of globally coupled Winfree oscillators using the Ott-Antonsen ansatz. Furthermore, we have deduced various bifurcation curves analytically from the reduced low-dimensional macroscopic variables for the exactly solvable case of the null value of the offset parameter. The analytical curves are found to agree well with the simulation boundaries of the phase diagram. We have also illustrated the finite-size effects on the nature of the dynamical states and bifurcation transitions.

ACKNOWLEDGMENTS

V.K.C. thanks DST, New Delhi for computational facilities under the DST-FIST programme (Grant No. SR/FST/PS-1/2020/135) to the Department of Physics. The work of V.K.C. is also supported by the SERB-DST-MATRICS Grant No. MTR/2018/000676 and CSIR-CRG Project under Grant No. CRG/2020/004353. M.M. thanks the Department of Science and Technology, Government of India, for providing financial support through an INSPIRE Fellowship No. DST/INSPIRE Fellowship/2019/IF190871.

[1] A. T. Winfree, J. Theor. Biol. **16**, 15 (1967).
[2] J. Buck, Quart. Rev. Biol. **63**, 265 (1988).
[3] A. T. Winfree, *The Geomentry of Biological Time* (Springer, New York, 1980).
[4] R. Gallego, E. Montbrio, and D. Pazo, Phys. Rev. E **96**, 042208 (2017).
[5] Joel T. Ariaratnam and S. H. Stroatz, Phys. Rev. Lett. **86**, 4278 (2001).

[6] F. Giannuzzi, D. Marinazzo, G. Nardulli, M. Pellicoro, and S. Stramaglia, Phys. Rev. E **75**, 051104 (2007).
[7] D. Pazó and E. Montbrió, Phys. Rev. X **4**, 011009 (2014).
[8] D. Pazo, E. Montbrio, and R. Gallego, J. Phys. A: Math. Theor. **52**, 154001 (2019).
[9] D. Golomb and D. Hensel, Neural Comput. **12**, 1095 (2000).
[10] G. B. Ermentrout and N. Kopell, SIAM J. Appl. Math. **50**, 125 (1990).
[11] R. E. Mirollo and S. H. Strogatz, SIAM. J. Appl. Math. **50**, 1645 (1990).
[12] J. Buck and E. Buck, Sci. Am. **234**, 74 (1976).
[13] Z. Néda, E. Ravasz, Y. Brechet, T. Vicsek, and A.-L. Barabási, Nature (London) **403**, 849 (2000).
[14] A. L. Hodgkin and A. F. Huxley, J. Physiol. **117**, 500 (1952).
[15] D. D. Quinn, R. H. Rand, and S. H. Strogatz, Phys. Rev. E **75**, 036218 (2007).
[16] L. Basnarkov and V. Urumov, J. Stat. Mech. (2009) P10014.
[17] E. Ott and T. M. Antonsen, Chaos **18**, 037113 (2008).
[18] E. Ott and T. M. Antonsen, Chaos **19**, 023117 (2009).
[19] C. S. Peskin, *Mathematical Aspects of Heart Physiology* (Courant Institute of Mathematical Sciences, New York, 1975), pp. 268–278.
[20] D. Pazó and R. Gallego, Chaos **30**, 073139 (2020).
[21] T. B. Luke, E. Barreto, and P. So, Neurak Comput. **25**, 3207 (2013).
[22] E. Ott, B. R. Hunt, and T. M. Antonsen, Chaos **21**, 025112 (2011).
[23] B. Ermentrout, *Simulating, Analyzing, and Animating Dynamical Systems: A Guide to XPPAUT for Researchers and Students* (Society for Industrial and Applied Mathematics, Philadelphia, 2002).
[24] S. Shinomoto and Y. Kuramoto, Prog. Theor. Phys. **75**, 1105 (1986).